Eur Biophys J (2002) 30: 588–604
DOI 10.1007/s00249-001-0187-x

ARTICLE

**Nikolai I. Kiskin · Rod Chillingworth
James A. McCray · David Piston · David Ogden**

The efficiency of two-photon photolysis of a "caged" fluorophore, *o*-1-(2-nitrophenyl)ethylpyranine, in relation to photodamage of synaptic terminals

Received: 24 May 2001 / Revised version: 3 September 2001 / Accepted: 3 September 2001 / Published online: 6 November 2001

Abstract Localized photolysis of caged neurotransmitters with the two-photon effect for investigations at synaptic preparations was evaluated by determining the toxicity to synaptic transmission of pulsed near-IR laser light focused into the terminals of the snake neuromuscular junction, and measuring the extent of photolysis of a conventional caging group with similar irradiation in microcuvette experiments. Photodamage was seen in synaptic terminals as a large, irreversible increase of spontaneous synaptic activity with laser flashes of 5 ms at 1 Hz at average powers > 5 mW and was due to multiphoton absorption. Localized photolysis due to two-photon absorption was investigated for a representative caged fluorophore, the 1-(2-nitrophenyl)ethyl ether of pyranine (NPE-HPTS). Irradiation of NPE-HPTS at 5 mW with the same optical arrangement produced very low rates of photolysis. NPE-HPTS photolysis mechanisms were investigated at high laser powers by measuring (1) the kinetics of two-photon fluorescence generated by two-photon photolysis in the focal volume and (2) the rates of HPTS accumulation inside closed 2–10 μm radius vesicles, measured with one-photon excitation during two-photon photolysis by repetitive 10 μs laser exposures. The two-photon cross-section of NPE-HPTS photolysis calculated from the rates is 0.02–0.04 GM (10^{-50} cm^4×s/photon) and limits the efficiency of photolysis at 5 mW. With free diffusional exchange, 50% steady-state cage depletion in the focal volume was estimated to occur only at high laser powers of ca. 72 mW, masked in experiments by multiphoton bleaching. Based on these results, the two-photon photolysis cross-section needed for 50% steady-state photolysis of a caged neurotransmitter at 5 mW is calculated as 31 GM, much higher than in existing caged compounds.

Keywords Multi-photon · Photolysis · Photodamage
Caged compounds · Synaptic transmission

Abbreviations *AOM*: acousto-optical modulator · *DIC*: differential interference contrast · *epp*: stimulus-evoked endplate potential · *FWHM*: full width of distribution at half of its maximum · *GC*: Gaussian cylinder function · *HPTS*: 8-hydroxypyrene-1,3,6-trisulfonate (or pyranine), fluorescent dye · *mepp*: spontaneous miniature endplate potential · *NA*: numerical aperture of objective · *NPE-HPTS*: *o*-1-(2-nitrophenyl)ethyl ether of HPTS, caged HPTS · *PMT*: photomultiplier

Introduction

Localized photolysis has potential interest for investigating mechanisms in synaptic transmission, particularly at inaccessible synapses of the CNS where high-resolution iontophoretic methods cannot be applied. To be useful, caged neurotransmitters need to be stable, pharmacologically inert, and release transmitters rapidly and efficiently on photolysis. It is important that photolysis is localized to the volume of a synapse, releasing small quantities of neurotransmitter that can be rapidly removed by endogenous mechanisms on the same timescale as a synaptic pulse. In experiments at the squid giant synapse, photolysis of a caged L-glutamate was produced with a near-UV flash lamp pulse, and although activation of the postsynaptic axon was rapid, generating a train of action potentials,

N.I. Kiskin[1] · R. Chillingworth · J.A. McCray[2]
D. Piston[3] · D. Ogden (✉)
National Institute for Medical Research, The Ridgeway,
Mill Hill, London NW7 1AA, UK
E-mail: dogden@nimr.mrc.ac.uk
Tel.: +44-20-89593666 ext 2003
Fax: +44-20-89064477

Present addresses:
[1]Physiologisches Institut der Universität Freiburg,
79104 Freiburg, Germany

[2]Department of Physics, Drexel University,
Philadelphia, PA 19104, USA

[3]Department of Biophysics, Vanderbilt University,
Nashville, TN 37232, USA

activation persisted for several hundred milliseconds, compared to the 2–3 ms associated with vesicular release localized to synaptic sites (Corrie et al. 1993). Similar fast but uncontrolled and persistent activation is seen when glutamate is released by photolysis in large (200 μm diameter) areas of cerebellar or hippocampal slices. With two-photon photolysis, both the time and spatial scales of synaptic activation should be reproduced and similar quantities of neurotransmitter or other agents generated. The dependence of the two-photon effect on the square of the light intensity makes the dimensions of the two-photon volume, with light focused by a high numerical aperture (NA) objective, comparable to single synaptic sites of dimensions of approximately 1 μm diameter and 50 nm cleft width. Thus localized two-photon photolysis of caged neurotransmitters can in principle be applied to mimic the action of neurotransmitters, to study the characteristics of postsynaptic processes, and more generally to study the action of endogenous molecules released in femtolitre volumes, intra- or extracellularly. However, despite this potential for localization, two-photon photolysis has not been applied to the study of single synaptic sites.

Two-photon photolysis for localized extracellular application of receptor ligands was implemented by Denk (1994) to map the cellular distribution of nicotinic receptors in a muscle cell line by scanning microscopy. Two-photon photolysis and photobleaching of a fluorophore were used by Svoboda et al. (1996) for characterization of diffusional coupling between dendritic spines of CA1 pyramidal neurones and the shaft, and two-photon photolysis of Ca^{2+}-loaded DM-nitrophen was applied to trigger artificial "Ca^{2+}-sparks" in cardiac myocytes (Lipp and Niggli 1998). Two-photon or multi-photon excitation requires high light intensities produced by far-red laser illumination with short, sub-picosecond pulses at around 10 ns intervals, with average power low enough for conventional microscope optics. However, for physiological experiments it is important to know the damage that can be produced by such irradiation in biological preparations in relation to the extent of photolysis. The very few reports of the successful use of multi-photon photolysis indicate that the method has problems of implementation.

In the experiments described here, the snake neuromuscular junction was used as an assay of synaptic photodamage. This preparation provides a single, well-defined, accessible synaptic connection in which individual presynaptic boutons can be clearly visualized. The junctions were exposed to the focused near-IR pulsed laser beam to assess the ability of synapses to sustain normal transmission during a representative experimental protocol in which the statistical parameters of transmission are studied.

An analysis of photolytic conversion and bleaching by the two-photon effect is based on theory described in the preceding article (Kiskin and Ogden 2001) and utilizes the fluorescence generated as pyranine (8-hydroxypyrene-1,3,6-trisulfonate, HPTS) is released from its caged form, the *o*-1-(2-nitrophenyl)ethyl ether (NPE-HPTS). This caged fluorophore has the same photolabile protecting group and properties as commonly used near-UV cages, NPE-caged ATP and NP-EGTA. In the present experiments, 640 nm laser light was used, close to the peak absorption predicted for near-UV cages.

Thus a direct comparison can be made of photolytic efficiency and laser damage to synaptic processes with the same illumination system, and the properties needed in a caged neurotransmitter utilizing the two-photon effect can be specified. The results show very little photolytic conversion even at laser powers which damage presynaptic terminals. Some of the results have been presented in abstract form (Kiskin et al. 1999).

Materials and methods

Laser photolysis apparatus

Photolysis and fluorescence were generated by two-photon excitation in a localized region of the microscope field and the specimen moved relative to the two-photon volume by a micrometer-driven stage. Pulsed laser light was from a Satori Model 774 Ultrafast Dye Laser (Coherent, Palo Alto, USA) capable of tuneable 100–400 fs duration light pulses at 76 MHz. The laser was pumped by 2–2.3 W frequency-doubled output (532 nm) of a mode-locked Antares 76-S Nd:YAG laser (Coherent, Palo Alto, USA). The kiton red/malachite green gain/saturating absorber dye combination for the Satori laser permitted a wavelength range of 605–655 nm with a maximum average output power of 90–150 mW. The wavelength used here was 640 nm. The laser beam was directed to an upright microscope (Zeiss Axioskop, Jena, Germany) by an acousto-optical modulator (AOM) (LM080, Isle Optics, Taunton, UK, lead molybdate crystal, analogue modulation) with a 0.3 μs measured rise time for switching, and also permitted adjustment of the power in the deflected beam. Pulse width was estimated by autocorrelation (FR-103 autocorrelator, Femtochrome Research, Palo Alto, USA). Optimal pulse width at the sample was achieved by changing the prism separation inside the Satori optical cavity and measuring the two-photon fluorescence of HPTS solution in the microscope focus. Maximal fluorescence at constant average power was achieved when pulse broadening due to a group delay dispersion of the optical elements between laser and specimen was compensated by pulse pre-chirp on the Satori output (Guild et al. 1997), in this case at a pre-chirped output pulse width of 340–360 fs. The pulse width was estimated as ~180–200 fs at the specimen after the AOM, the predominant dispersive element in our system. A 3× beam expander (Melles Griot, Cambridge, UK) was used to centre the laser focus on the optical axis relative to the image plane and decrease the spot size. The laser beam was directed through the epifluorescence port of the microscope (optical elements removed) via a band-reflecting (550–700 nm) dichroic mirror to the water immersion objective (Zeiss Achroplan, 40×W, 0.75 NA). Input powers were measured entering the microscope and corrected to average powers at the specimen (quoted in the paper), taking into account 60% transmission of 640 nm light measured for the optical system described above. In vesicle and muscle fibre experiments, single-photon excitation of fluorescence and photolysis were via a 490 nm dichroic mirror mounted in an additional piggyback epifluorescence unit above the standard epifluorescence port, with the excitation monochromator (TILL Photonics).

Photolysis procedures and fluorescence measurements

Solutions

The trisodium salt of HPTS was obtained from Molecular Probes (Eugene, USA). Caged HPTS, the *o*-1-(2-nitrophenyl)ethyl ether of HPTS, was synthesized from HPTS as described (Jasuja et al. 1999). HPTS and NPE-HPTS were dissolved either in Na-borate buffer (50–100 mM, pH 9) or 100 mM HEPES-Na solution (pH 7 or pH 6) with the addition of 5 mM reduced glutathione (Sigma, Poole, UK).

Microcuvette experiments

Two procedures were used for photolysis calibration using different fluorescence excitation. In the first, photolysis and fluorescence excitation were two-photon, produced with pulsed laser illumination of solutions in 100 μm pathlength rectangular section microcuvettes (Camlab, Cambridge, UK), sealed with grease at both ends and placed under a water immersion objective in the laser focus. The fluorescence of photolysed NPE-HPTS was recorded by two-photon excitation from the laser spot during 4.4 ms trains of laser pulses at constant average power in range 12–72 mW, delivered at 150–500 ms intervals to allow diffusional re-equilibration of products in the cuvette between the pulse trains. The emission filter was 540 nm, 10 nm bandwidth. Epifluorescence was collected with a side-window photomultiplier (PMT) (R4220P, Hamamatsu Photonics, Enfield, UK) connected to a photon-counting SR430 multi-channel scaler with a SR445 5× pre-amplifier (time/bin resolution 640 ns, saturation at $\sim 2\times10^7$ counts/s; Stanford Research Systems, Sunnyvale, USA). The timecourse of the fluorescence increase at each laser power was averaged by accumulation of PMT counts in 640 ns bins for 1000–20,000 exposures synchronized with the laser illumination. Background fluorescence in the cuvette outside the two-photon spot was not changed after many repeated measurements, indicating that the cuvette volume was large enough that errors due to this source were negligible. Saturation of photon counts at high levels of fluorescence was avoided by inserting 1% or 10% transmission neutral density filters in the emission path. A photolysed solution for two-photon fluorescence calibrations was made by complete near-UV photolysis of cuvette solutions of the same composition as those used for two-photon photolysis. This was achieved with 20–50 flashes of a xenon flash lamp (Rapp Optoelektronik, Hamburg, Germany).

Vesicle experiments

In the second procedure, two-photon photolysis was produced in 2–10 μm radius closed aqueous vesicles formed in Sylgard resin 184 (Dow Corning) on a cover glass, and one-photon fluorescence excitation used to measure total fluorescence accumulated in the vesicle. Vesicles were made by dispersing 2–10 μL of NPE-HPTS solution in 50–100 μL Sylgard, placing 10–20 μL of mixture on a cover glass, allowing air bubbles to disperse and curing on a 60 °C hotplate (with a cover to retain heat) for 7 min. The timecourse of accumulation of total fluorescence in the vesicle was measured with a Imago cooled CCD camera (TILL Photonics, Munich, Germany) during 500–10,000 laser exposures, emission filter 515–565 nm wideband, excitation set to 460 nm. 10 μs laser flashes were used to minimize the influence of cage depletion from the two-photon spot and were separated by 100–200 ms to allow completion of the photochemical reaction and diffusional re-equilibration of reagents within the vesicle. To reduce the errors caused by HPTS bleaching, photolysis was allowed to go to approximately 10% of the final vesicle fluorescence level, determined at the end by complete photolysis of the same vesicle with 7–12 min exposure to 340 nm monochromator light via the epifluorescence system and microscope objective. Vesicle diameter was measured from CCD images.

Curve fitting

Models were fitted to data sets with Levenberg-Marquardt nonlinear least squares optimization of parameters in Origin 5.0 (Microcal Software, Northampton, USA).

Experiments at the snake skeletal neuromuscular junction

Experiments to test the effects of irradiation on synaptic transmission were made with costo-cutaneous muscles of the garter snake *Thamnophis sirtalis*. Snakes were killed by concussion and destruction of the brain. Ringer solution contained 147 or 110 mM NaCl, 20 or 50 mM HEPES, 2.0 mM KCl, 2 mM $CaCl_2$ and 1 mM $MgSO_4$, buffered to pH 7.2 with NaOH. In most experiments the presynaptic terminals were stained by incubating the muscle for 5–10 min in a solution containing 2 μM FM 1-43 (Molecular Probes), 2 mM $CaCl_2$, 15 mM KCl replacing equivalent NaCl, and in some experiments 10 μM (+)-tubocurarine. After staining, muscles were washed extensively in normal Ringer solution until transmission was restored. Fluorescent staining was viewed by a cooled CCD at 515–565 nm, with excitation at 460 nm. The two-photon spot was carefully aligned with the specimen plane at a predetermined point in the field seen by the CCD chip, by means of point intensity measurements on the image of a cover glass coated with fluorescent beads (0.28 μm fluoresceine microspheres; Polysciences, Warrington, USA), or in fluorescent HPTS solution. The microscope stage and micromanipulators were mounted on a bearing plate that could be moved by micrometers under visual control to place any point of the specimen in the two-photon volume. The nerve was stimulated with 0.1 ms constant current supramaximal shocks 5× threshold at 1 Hz. Quantal content of the evoked endplate potentials (epps) was adjusted to give approximately 50% failures by varying the external Ca^{2+} and Mg^{2+} concentrations, usually 0.1 mM Ca^{2+}, 2 mM Mg^{2+}. The protocol was to stimulate at 1 Hz while recording from the junctional region of a twitch fibre epps and spontaneous miniature epps (mepps) at room temperature (21 °C) with conventional microelectrodes of resistance 7–30 MΩ when filled with 2 M KCl (Axoclamp 2 A amplifier, Axon Instruments, Foster City, USA). A single bouton placed in the two-photon volume was irradiated with pulsed laser light at various intensities. Laser exposures of 1–10 ms were timed to precede and coincide with the rise of the epp to ensure the terminal was irradiated during the transmitter release. The experimental timing and data capture were done with Spike 2 software and 1401plus interface (CED, Cambridge, UK); data were recorded in parallel on FM tape. The rate and timing of mepps were determined off-line with template fitting functions of Spike 2 and subsequent inspection and correction.

The dimensions of the two-photon volume

The rates of two-photon photolysis in the focus of a laser beam depend on the distribution of the squared light intensity, which is non-uniform and peaks in the small region described as the two-photon volume. For a Gaussian-shaped laser beam, with $1/e^2$ waist radius w_0 and wavelength λ propagating in water (refractive index $n_0 = 1.33$), the intensity, I, of light focused by an underfilled objective is described by a Gaussian-Lorentzian function. The probability of observing two-photon absorption is proportional to the square of the intensity and depends on radius r, axial distance z from the focus and total power P as:

$$I(r,z)^2 = \frac{4P^2}{\pi^2 w_0^4\left[1+(z/Z_R)^2\right]^2} exp\left\{-\frac{4r^2}{w_0^2\left[1+(z/Z_R)^2\right]}\right\} = \frac{4P^2}{\pi^2 w_0^4} S(r,z)^2 \quad (1)$$

Here $Z_R = \pi {w_0}^2 n_0/\lambda$ is the Rayleigh length and $S(r,z)$ is defined as a unitless spatial distribution function having maximal value

$S(0,0) = 1$ at $r = 0$, $z = 0$ (Xu and Webb 1997). The value of w_0 was estimated from recordings of two-photon fluorescence integrated over the laser spot during Z-scans made with a piezo-driven objective focus through a glass coverslip, either in bulk fluorophore-containing solution or through a thin film of fluorophore deposited on the coverslip. Least squares estimates of w_0 were obtained by fitting the integrated fluorescence as a function of axial distance z, and independently from the sectional radii obtained by CCD imaging. Both measurements gave a beam waist of $w_0 = 0.7$ μm, in turn giving $Z_R = 3.20$ μm. The intensity profile of the two-photon volume $S(r,z)^2$ calculated from Eq. (1) has a full width of distribution at half of its maximum (FWHM) of 0.58 μm in the focal plane and 4.1 μm axially. These procedures also allowed the position of the laser beam focus to be adjusted relative to the image. For $w_0 = 0.7$ μm and $\lambda = 640$ nm, the total two-photon fluorescence in an infinite medium will be collected from the effective spot volume V_s defined for a Gaussian-Lorentzian beam as:

$$V_s = 2\pi \int_{-\infty}^{\infty} \int_{0}^{\infty} S(r,z)^2 r \mathrm{d}r \mathrm{d}z = \frac{n_0 \pi^3 w_0^4}{4\lambda} = 3.87\ \mu\mathrm{m}^3 \qquad (2)$$

The spot volume was used below in calculating the correction factor applied to the rate of fluorescence accumulation during photolysis of NPE-HPTS in closed vesicles.

Results

Laser damage in synaptic terminals of the snake muscle endplate

Damage produced by pulsed near-IR laser illumination in a synaptic preparation was assessed physiologically and morphologically at the motor endplates of twitch fibres of costo-cutaneous muscles from the garter snake. Figure 1A shows images obtained with differential interference contrast (DIC) and with epifluorescence from the same preparation stained with the presynaptic vesicle marker FM 1-43 (Betz and Bewick 1992). The relative dimensions of the two-photon spot and presynaptic bouton are shown by the epifluorescence image of another endplate and of the two-photon spot at the same scale in Fig. 1B. The region illuminated by the laser was smaller than individual synaptic boutons. Care was taken to align the bouton so that the laser spot was centrally located and parfocal with the image. A protocol of stimulation and illumination typical of a physiological experiment at a synaptic preparation was followed. Microelectrode recordings were made adjacent to the endplate. The nerve was stimulated at 1 Hz with 0.1 ms supramaximal shocks at 5× threshold intensity, determined from the twitch response before impalement, and the proportion of failures was adjusted to about 50% with low Ca^{2+} Ringer solution, usually 0.1 mM Ca, 2 mM Mg. The laser illumination was applied as a pulse of 1, 5 or 10 ms duration to coincide with the presynaptic action potential and rise of the epp, as indicated for 5 ms and 1 ms pulses in Fig. 1C. Several hundred stimuli were given in control and laser illuminated synapses, and the effects of damage were assessed from changes in the mepp frequency, statistical parameters of transmission, and from morphological changes.

The sign of synaptic disruption was a large increase in the frequency of mepps following successive laser pulses. The effect is illustrated in Fig. 1D, which shows continuous records of mepp frequency from an endplate in which three boutons were successively illuminated with different intensities and pulse durations. In bouton 1 (Fig. 1B, left panel), the mepp frequency was stable at 0–5 s^{-1} for 900 s without illumination, including two periods of 200 nerve stimulations at 1 Hz. Laser exposure for a further three periods of 200 3.6 mW, 5 ms pulses during stimulation with the same protocol resulted in little or no increase of mepp frequency. From this baseline a second bouton (Fig. 1B, right panel) was exposed to 5× higher power of 18 mW but of 1 ms duration, keeping the same photon dose. After two periods of 200 pulses the effect was a large increase in the mepp frequency to 20 s^{-1}. Exposure of a third bouton at the same endplate to the same illumination increased the mepp frequency further by a similar extent to about 40 s^{-1}. Generally, the increase reversed very slowly, in 15–60 min, possibly as a result of vesicle depletion from the damaged bouton. It is likely that the damage effects were at a single bouton, whereas the mepps arise from the many release sites at each endplate (indicated by the maximum quantal content of >200; Fiekers 1983). Thus, the control mepp frequency at a single bouton would be very low, on the order of 0.01 Hz, and the frequency increase due to selective damage at the illuminated bouton is therefore very much larger in proportion to control than indicated by the numbers recorded. The results from a total of 22 boutons are summarized as follows, an increased mepp rate counted positive when maintained at >10 s^{-1}:

1. 3 or 3.6 mW, 5 ms: no frequency increase in 3/3 boutons in 600–1200 pulses.
2. 6 mW, 5 ms: no frequency increase in 3/6 after 400–600 pulses; frequency increase in 3/6 in 60–300 pulses.
3. 12 mW, 5 ms: frequency increase in 5/5 after 90–170 pulses.
4. 18 mW, 5 ms: frequency increase in 3/3 after 60–300 pulses.
5. 18 mW, 1 ms: frequency increase in 2/2 after 350–400 pulses.
6. 30 mW, 1 ms: frequency increase in 3/3 after 130–180 pulses.

The average power producing damage at 5 ms exposure in 50% of experiments after about 500 pulses was 6 mW; lower average power appeared not to produce a mepp frequency increase in more than 600 pulses. Higher average powers produced damage within about 100 pulses, even when the duration was reduced to keep the total energy exposure the same, e.g. compare 3.6 mW, 5 ms and 18 mW, 1 ms; 6 mW, 5 ms; and 30 mW, 1 ms. Furthermore, the data indicate that the total exposure time (number of pulses multiplied by pulse duration) required to induce damage depends inversely on the square of the average power. Both

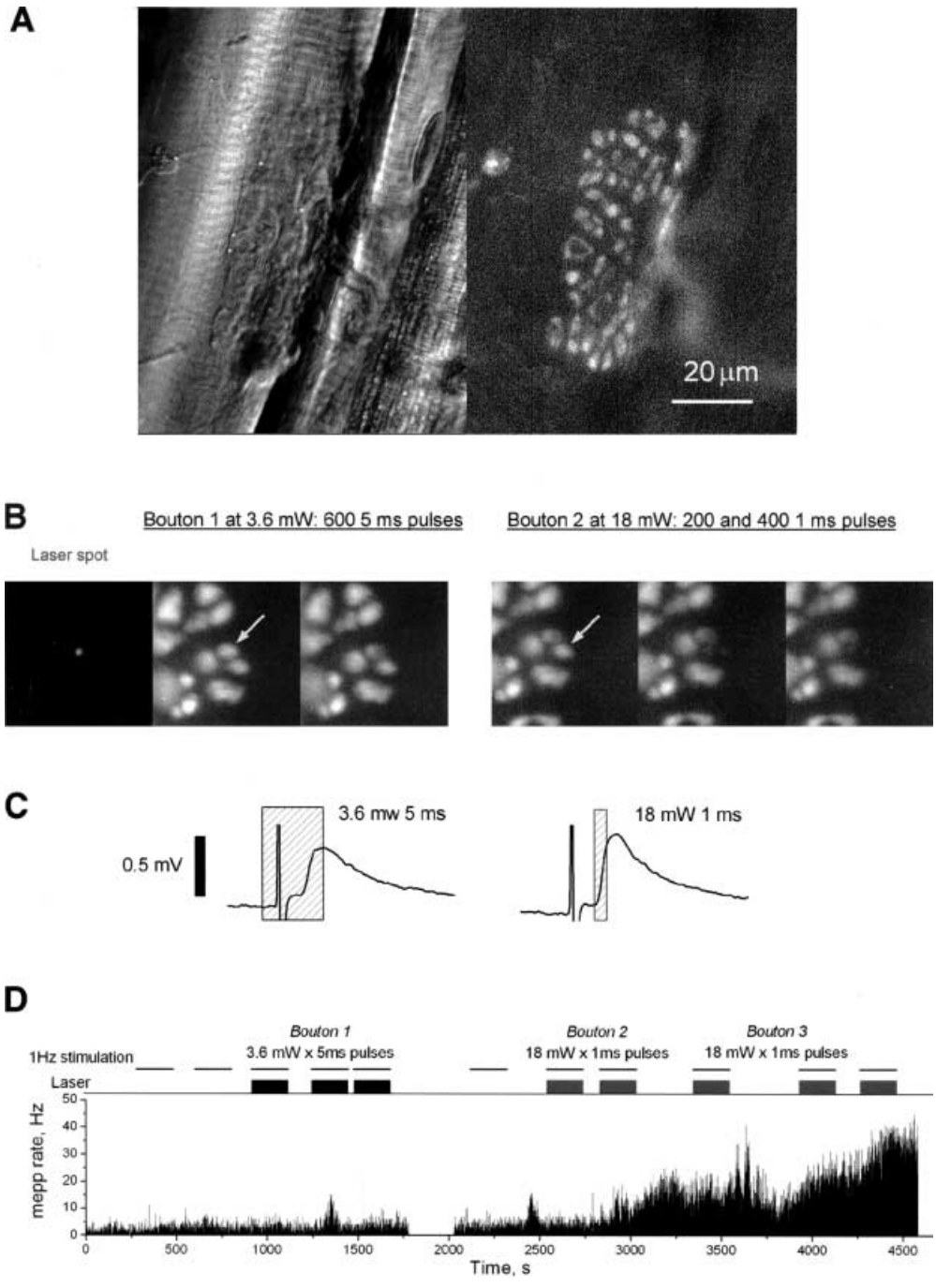

Fig. 1A–D Morphological and physiological evidence of photodamage at the snake neuromuscular junction. **A** DIC (*left*) and epifluorescence (*right*, 460 nm excitation, 520–560 nm emission) images of an endplate on a costo-cutaneous muscle stained with FM1-43. Scale bar 20 μm. **B** High-power images at the same magnification of the two-photon laser spot focused in a film of fluorescent beads (26×26 μm field, excitation 640 nm, emission 500–550 nm) and an endplate stained with FM1-43 (excitation 460 nm). *Arrows* indicate two control images of boutons placed in the centre of the field before illumination by the laser. The timing of other images corresponds to a mepp record from the same endplate shown in **D**. **C** Endplate potentials recorded in two fibres showing the relation of synaptic events to the periods of illumination by laser pulses of long (5 ms) and short (1 ms) duration. **D** Continuous record of a mepp frequency during an experiment in which three different boutons at a single endplate (shown in **B**) were used to test the effects of laser illumination. Two periods of control nerve stimulation, 200 stimuli at 1 Hz (*thin bars*), were followed by three periods of stimulation combined with irradiation at 3.6 mW and 5 ms duration (*thick bars*) in the first bouton. Two more boutons at the same endplate were tested with control stimulation, then 2–3 periods of irradiation at 18 mW with 1 ms laser pulses. The bin width for the mepps count was 1 s

observations are consistent with a multi-photon effect producing damage in the presynaptic terminal. No change was detected in the probability of failures of transmission at the whole endplate, indicating that there was no large enhancement of transmission at the exposed bouton, but not ruling out the possibility of a *decrease* of release probability at the irradiated bouton. Thus, a practical upper limit of irradiation from the 200 fs, 76 MHz pulsed laser at 640 nm in this synaptic preparation is 5 mW average power with 5 ms exposures, permitting for experimental purposes 1 Hz exposure frequency for more than 10 min.

There was no effect on muscle fibre membrane potential that could be attributed to the laser exposure described above. However, in earlier experiments in frog muscle, continuous 1 s exposures to 25 mW average power produced membrane rupture. Finally, both innocuous and damaging levels of illumination produced bleaching of FM1-43 in boutons, with over 600 exposures at low intensity (3.6 mW, 5 ms; Fig. 1B left panel) and more quickly and completely at higher intensities. The fluorescence was depleted from the whole bouton, including the areas outside the small illuminated two-photon spot (Fig. 1B, right panel), indicating cycling of

stained vesicles through the bouton even at very low release probability at individual sites (estimated $P << 0.01$).

Two-photon photolysis of NPE-HPTS

The rate of photolysis of NPE-HPTS by the two-photon effect, releasing the fluorophore HPTS, was studied by recording the fluorescence with excitation either by two-photon excitation in the spot by the pulsed laser, or by one-photon excitation of fluorescence accumulated in the limited volume of 4–20 μm diameter aqueous vesicles. In the first method the kinetics of photolysis were estimated with free diffusional exchange of all the reactants (NPE-HPTS, photolysis intermediates and products) between the two-photon spot and the surrounding bulk solution. In the second, the rate of two-photon photolysis was measured from the rate of accumulation in the vesicle of one-photon fluorescence corrected by the ratio of vesicle volume to two-photon volume to yield the rate of photolysis.

Measurements in the two-photon spot

The fluorophore generated by NPE-HPTS photolysis in the laser spot was excited by two-photon absorption during exposure to 4.4 ms trains of laser pulses. Fluorescence was generated during exposure of 0.5, 2 and 5 mM solutions of NPE-HPTS in microcuvettes at laser powers greater than 18–24 mW, and the rate and amplitude increased when the laser light intensity was increased. Representative records are shown in Fig. 2.

At all laser powers shown, a small initial step of fluorescence was seen immediately after switching on the laser pulse (Fig. 2, bottom traces). The amplitude of the step was small, $1.2 \pm 0.6\%$ of the fluorescence recorded at the same power after complete photolysis of the same solution. The possibility that the initial step was due to rapid photolysis occurring instantaneously on laser exposure was tested by monitoring two-photon fluorescence of the released product with a low intensity test excitation (3–5 mW) immediately after a brief (10 μs) exposure to a high-intensity photolysis pulse (Brown et al. 1999). No appreciable additional fluorescent "tail" of diffusing products was seen following a single brief 10 μs high-intensity exposure, indicating that no initial rapid photolysis had occurred (records not shown). In contrast, following long (20 μs to 1 ms) high-intensity photolysing pulses, a transient elevated fluorescence was seen upon switching to the low-intensity test pulse. The initial amplitude of the transient test fluorescence was greater when it followed high-intensity or long duration photolysis pulses. Plots of the initial amplitude of the test pulse against the duration of the preceding photolysis pulse showed a monotonic increase from near zero at 10 μs. This indicates a continuous accumulation of fluorescence due to a constant photolysis rate during the high-intensity pulse, rather than a high but transient photolysis rate at the beginning of the photolysis pulse. Thus, the initial fluorescence on laser exposure was due to a background fluorescence of NPE-HPTS or to HPTS impurities rather than to fast photolysis at the very beginning of illumination.

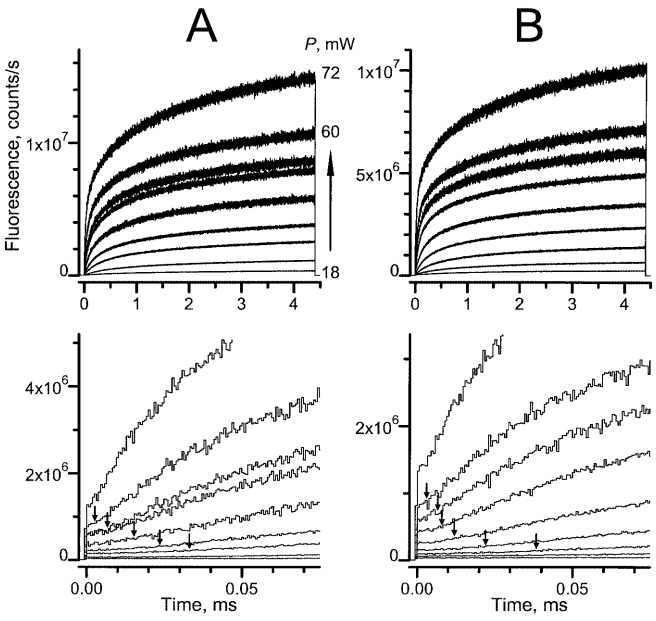

Fig. 2A, B Fluorescence traces recorded from the laser spot during photolysis of NPE-HPTS by 4.4 ms laser exposures. NPE-HPTS concentrations were 2 mM at pH 9 (**A**) and 5 mM at pH 7 (**B**). Traces were recorded at average laser powers from 18 to 60 mW (increasing from bottom in 6 mW intervals, powers estimated at the specimen) and 72 mW (*top traces*). Each trace is averaged from 2000 to 20,000 laser exposures of 4.4 ms duration at 100–250 ms intervals. The *upper panels* show the full photolysing pulse duration (4.4 ms), the *lower panels* the first 75 μs to show initial delays (points of inflection indicated by *arrows*) of rise of fluorescence. The vertical scales are different for **A** and **B**, and expanded by the same proportion in the lower panels. The photon counting bin width of 640 ns can be seen in the lower records

A 4.4 ms laser exposure (Fig. 2) showed no detectable photolysis at average powers up to 12 mW. Only the initial step increase of fluorescence was observed. At higher powers a subsequent rise of fluorescence was seen during the pulse. In the range 30–60 mW the fluorescence rose with a delay after the light was switched on, seen as an inflection (indicated by arrows) in the lower records of Fig. 2. These delays decreased markedly from ~50–100 μs at 30 mW average power to a few microseconds at 60–72 mW. Thus the fluorescence increase due to photolysis showed sigmoidal initial kinetics. On a slower, millisecond timescale (Fig. 2, top) the fast increases in fluorescence during the first 200–500 μs were followed by a slower increase, and the fluorescence recorded from the spot was close to a steady state after 4.4 ms. Comparison of the fluorescence traces obtained at pH 9 and pH 7 (Fig. 2A and B) shows that the pH did not cause any obvious difference in the kinetics of the fluorescence rise, and thus in the rates of photolysis.

The fluorescence increase seen at high laser power is due to greater photolysis *and* enhanced excitation of fluorescence. To account for the enhanced two-photon excitation, photolysis traces were normalized to the peak amplitudes of fluorescence observed at the same laser power in the same solutions after NPE-HPTS was completely photolysed by a xenon flash lamp (during normalization the initial fluorescence in photolysis traces was subtracted from both values). To illustrate the effects of increased excitation alone, fluorescence records from photolysed NPE-HPTS solutions are shown in Fig. 3A for different laser powers (12–72 mW, 2 mM NPE-HPTS solution completely photolysed by xenon lamp, pH 9). At laser powers exceeding 24 mW, the fluorescence showed a fast decline during the first 20–100 μs, then a slower decline to a steady level, due to fluorophore bleaching at these powers. The dependence of initial peak fluorescence on the average power at the sample, P, was plotted in double-logarithmic coordinates for several concentrations of photolysed NPE-HPTS, shown in Fig. 3B. The slopes of fitted regression lines were $n = 1.93 \pm 0.11$, 1.85 ± 0.03, 1.91 ± 0.10 and 1.95 ± 0.03 for different concentrations. This indicates that the peak fluorescence was proportional to the square of the average power, P^2, i.e. was due to two-photon excitation of the products of NPE-HPTS photolysis. Peak two-photon fluorescence at a given laser power was proportional to the initial cage concentration, and for photolysed 5 mM NPE-HPTS solutions it was on average 2.31 ± 0.38 times brighter at pH 9 than at pH 7 (data for $P < 60$ mW). For high powers, 60–72 mW, minor deviations were seen towards lower peak values and may have been due to bleaching at the onset of illumination (~0.6 μs) or some loss of PMT counts due to saturation.

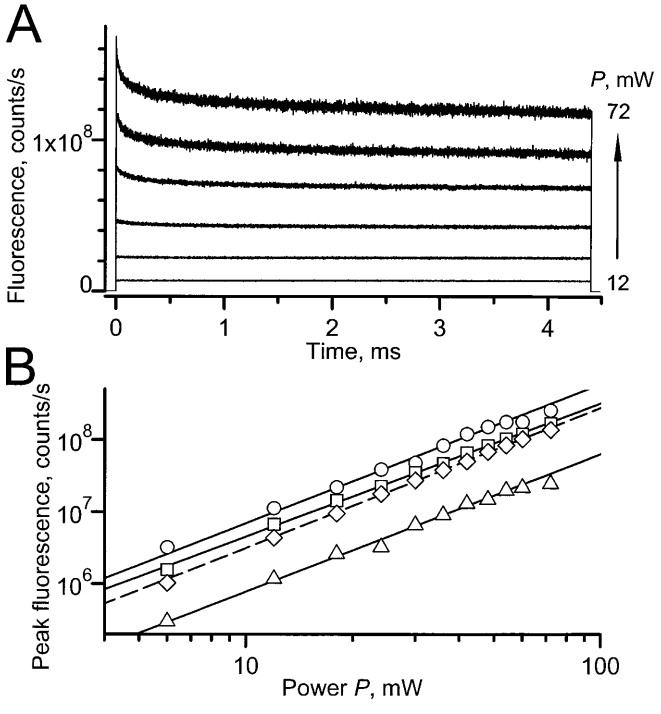

Fig. 3A, B Timecourse and amplitude of fluorescence of photolysed NPE-HPTS solutions at different average laser powers. NPE-HPTS solutions were photolysed by a xenon flash lamp to yield fluorescent products, presumably mostly HPTS, and non-fluorescent by-products. **A** Fluorescence emitted at 540 nm by 2 mM photolysed NPE-HPTS solution (pH 9.0) with excitation in the laser spot by 200 fs pulses of 640 nm light at average powers from 12 to 72 mW (increasing from the bottom trace in 12 mW intervals). **B** Dependence of peak fluorescence of photolysed NPE-HPTS solutions on laser power. Least-square fits of peak fluorescence at powers $P \leq 54$ mW to a γP^n model are superimposed. *Solid lines* represent fits to the data at pH 9, *dashed line* at pH 7. Best fit estimates at pH 9: 5 mM (*circles*), $\gamma = 8.19 \pm 3.31 \times 10^4$, $n = 1.93 \pm 0.11$; 2 mM (*squares*), $\gamma = 6.44 \pm 0.77 \times 10^4$, $n = 1.85 \pm 0.03$; 0.5 mM (*triangles*), $\gamma = 9.54 \pm 3.51 \times 10^3$, $n = 1.91 \pm 0.10$. At pH 7: 5 mM (*diamonds*, *dashed line*), $\gamma = 3.58 \pm 0.43 \times 10^4$, $n = 1.95 \pm 0.03$

The initial slopes of normalized photolysis traces increased strongly with increased laser power over the range 12–72 mW (Fig. 4A) and were used to estimate the photolysis rate constants. It is necessary to take account of the non-uniform distribution of the light intensity, $S(r,z)^2$, in the GL spot (Eq. 1). A Gaussian cylinder (GC) provides a good geometric approximation $F(r,z)$ to the distribution of light intensity in the spot $S(r,z)^2$, and has been used in a similar approach with diffraction-limited spot geometry by Brown et al. (1999):

$$F(r,z) = exp\left(-r^2/w_R^2\right) exp\left(-z^2/w_Z^2\right) \quad (3)$$

where the GC parameters w_R and w_Z can be defined such that FWHM values for $F(r,z)$ in Eq. (3) are equal to those for $S(r,z)^2$ for the GL beam with measured waist $w_0 = 0.7$ μm and at $\lambda = 640$ nm. From Eqs. (1) and (3), assuming $z < Z_R$ near the focus, the waist radius of the GC required in the focal plane is $w_R = w_0/2 = 0.35$ μm. The axial waist of the GC matching the FWHM of $S(r,z)^2$ on the z-axis is $w_Z = 0.773$, $Z_R = 2.47$ μm. These values were used in evaluating the initial kinetics of the fluorescence change due to photolysis, assuming a constant rate of photolysis proportional to the squared intensity at each point and taking account of diffusional redistribution of the fluorescent product in an infinite medium. The GC model is described in detail in Appendix 2. Since the peak fluorescence was used for normalization, the bleaching seen at high laser powers will be present in the normalized traces. However, as bleaching is small at powers up to 36 mW, and fluorescence generation during photolysis is the primary process, the contribution of bleaching to the initial kinetics was neglected. Importantly, by taking the model with a constant rate of photolysis, cage depletion in the laser spot was also assumed negligible. Thus, owing to these two factors, only the initial photolysis kinetics could be fitted. For a diffusion coefficient for free HPTS of $D = 230$ μm^2/s (at 24 °C; Xia et el. 1998) and the same value assumed for NPE-HPTS, with $w_R = 0.35$ μm and $w_Z = 2.47$ μm, values of the corresponding diffusional times, $\tau_R = {w_R}^2/D$ and $\tau_Z = {w_Z}^2/D$, were 0.533 ms and 26.6 ms, respectively. These parameters were used in Eq. A10 (Appendix 2) to estimate the rate constant by

non-linear least squares fitting to the initial parts of the normalized photolysis curves. For each set of measurements at a given NPE-HPTS concentration and pH, a set of values of the photolysis rate constant $k(P)$ was found as a function of the average laser power P (fitted curves indicated by lines in Fig. 4A). At low laser powers, allowance was made for the initial delays by choosing the interval for fitting at a later time, and at high powers only the initial part of curves could be reliably fitted with the GC model, due to the combined effect of bleaching and cage depletion.

Dependence on power

The dependence of the apparent photolysis rate constant on light intensity can be seen in plots of the initial rate constant, $k(P)$, against average power, P, shown in Fig. 5A. For clarity the data are represented in double-logarithmic coordinates by mean values and standard deviations at each power, and are shown for pH 7 and pH 9. Data at each pH were fitted by least squares to $k(P)=\gamma P^n$. Best fit values of n were 2.31 ± 0.16 at pH 9

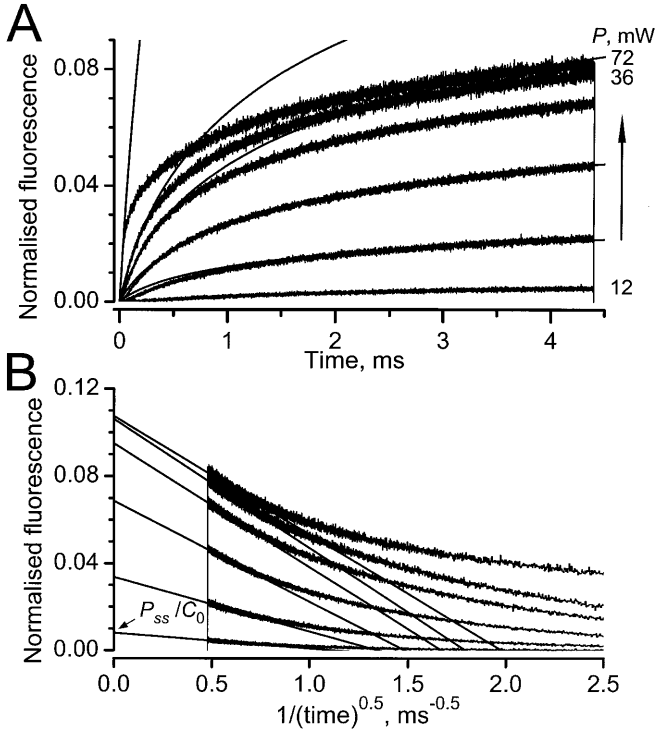

Fig. 4 Analysis of initial kinetics (**A**) and of approach to the steady state (**B**) for two-photon fluorescence obtained during photolysis of 2 mM NPE-HPTS at pH 9 and laser powers from 12 to 36 mW (shown at 6 mW intervals) and 72 mW (*top trace*). Each trace was normalized by peak fluorescence at that laser power after all NPE-HPTS in the microcuvette was photolysed with a xenon arc flash lamp (data points in Fig. 3B). Initial "steps" of fluorescence seen immediately on laser exposure before photolysis (Fig. 2, bottom panels) were subtracted before normalization. **A** Smooth lines are least-squares fits to initial rates of photolysis, evaluated on the initial region of the data using equation (A10) (Appendix 2), which assumes continuous release at a constant rate from a source with GC geometry. Diffusional parameters, $\tau_R=0.533$ ms and $\tau_Z=26.6$ ms, were calculated assuming a diffusion coefficient for HPTS of 230 μm^2/s. **B** Steady-state levels of fluorescence were evaluated by plotting normalized fluorescence in $t^{-0.5}$ coordinates and fitting the data at $t>1.75$ ms by regression lines. The normalized steady-state levels of fluorescence, P_{ss}/C_0, are given by intercepts with the ordinate as $t^{-0.5}\rightarrow0$ (indicated by *arrow* at 12 mW)

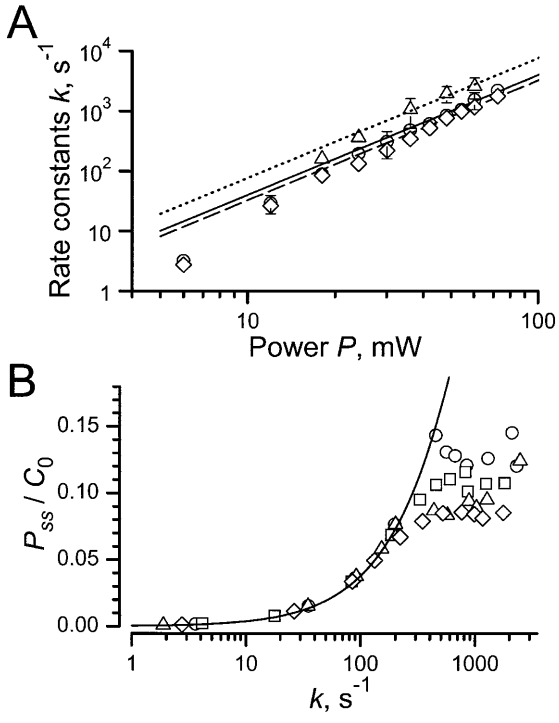

Fig. 5A, B Photolysis rate constants and steady-state fluorescence for two-photon photolysis of NPE-HPTS. **A** Rate constants of NPE-HPTS photolysis plotted as a function of the laser power. Summary of data from the laser spot and from photolysis in 5–20 μm vesicles. For clarity, mean values over different concentrations at each laser power are shown, and line fitting performed for whole data sets. *Points* represent means of initial rates obtained by fitting data recorded from the laser spot as shown in Fig. 4A. NPE-HPTS concentrations were 0.5, 2 and 5 mM at pH 9 (*circles*), 5 mM at pH 7 (*diamonds*). Mean photolysis rates estimated from fluorescence accumulated in vesicles are shown (*triangles*, 0.5 mM NPE-HPTS, pH 9). *Vertical bars* show standard deviations where they exceeded the size of symbols. Data points were fitted with a γP^n model and in unconstrained fits (not shown) gave estimates for n: 2.31 ± 0.16 (*circles*), 2.24 ± 0.06 (*diamonds*) and 1.92 ± 0.30 (*triangles*). *Straight lines* are the fits to all data points constrained with "power-square", $n=2$; estimated values of γ (in s^{-1} mW^{-2}) were 0.402 ± 0.013 at pH 9 (*solid line*), 0.327 ± 0.006 at pH 7 (*dashed line*) and 0.770 ± 0.052 for the rate constants measured in vesicles (*dotted line*). **B** Normalized steady-state fluorescence of product, P_{ss}/C_0 (see Fig. 4B), plotted as a function of rate constants k of NPE-HPTS photolysis obtained from GC fits in measurements from the spot as shown in Fig. 4A; semi-logarithmic scale. Data for NPE-HPTS at pH 9 at concentrations of 5 mM (*circles*), 2 mM (*squares*) and 0.5 mM (*triangles*), and at pH 7 for 5 mM NPE-HPTS (*diamonds*). *Solid line*: data at laser powers producing negligible bleaching ($k\leq300$ s^{-1}, pH 9) were fitted with a hyperbolic relation predicted for average concentration of product normalized to the initial cage concentration, as a function of the photolysis rate constant, k, for a single photolysis step inside a sphere in an infinite medium, $P_{ss}/C_0=k/(k+K_{0.5})$ (Eq. 4 in text; see Kiskin and Ogden 2001). The best fit, with the maximum constrained to 1.0, was obtained with $K_{0.5}=2530\pm55$ s^{-1}

and 2.24 ± 0.06 at pH 7 (fits not shown). These values are close to 2, indicating that the initial rates were proportional to the square of the average laser power, consistent with a two-photon absorption underlying photolysis. Constraining the slope to $n = 2$ gave estimates of the coefficients: $\gamma = 0.402 \pm 0.013$ s^{-1} mW^{-2} at pH 9 and $\gamma = 0.327 \pm 0.006$ s^{-1} mW^{-2} at pH 7 (shown in Fig. 5A by solid and dashed lines, respectively). Significant deviations from the power-square dependence were seen only at laser powers ≤ 12 mW, where the delays in the fluorescence increase were large (see Fig. 2A, bottom trace). At intermediate laser powers (12–30 mW, e.g. 24 mW in Fig. 4A) the fits of the GC model to the fluorescence timecourse were good: values of k fitted to the initial parts of the trace closely predicted the subsequent experimental fluorescence curves over the whole duration of exposure.

Dependence on pH

The overall rate of photolysis of NPE-HPTS by near-UV irradiation strongly increases on lowering the pH, with rates of 16 s^{-1} at pH 9, 550 s^{-1} at pH 7, 6900 s^{-1} at pH 6 and $>35{,}000$ s^{-1} at pH 5 (Jasuja et al. 1999). However, two-photon photolysis of NPE-HPTS proceeded with similar rates at pH 7 and pH 9 (Figs. 2 and 5A). The effect of pH was investigated further by comparing two-photon NPE-HPTS photolysis in similar experiments at pH 6.0 and pH 9.0. No differences in the rates of photolysis between pH 6 and 9 were seen at each power (data not shown). Thus, in contrast to data with near-UV photolysis, rates of NPE-HPTS photolysis generated by the two-photon effect and monitored with two-photon excitation in the laser spot showed no dependence on pH in the range 6–9. The absolute fluorescence intensity recorded from a photolysed solution at pH 6 was less than at pH 9.

Steady-state fluorescence levels

The steady-state concentration of photolysis products in the laser spot at each intensity depends not only on the rate of photolysis but also on the diffusional exchange of cage, intermediates and products with the bulk solution. For a simplified model of a single irreversible reaction and a spherical focal volume in a bulk medium of cage concentration C_0, the dependence of the steady-state product concentration, P_{ss}, on the photolysis rate constant, k, is hyperbolic with the half-maximum, $K_{0.5}$, determined by the radius of the sphere and the diffusion coefficient of the reactants (Kiskin and Ogden 2001):

$$P_{ss} = \frac{C_0}{1 + K_{0.5}/k} \tag{4}$$

where $K_{0.5} = 2.5D/A^2$, D is the diffusion coefficient assumed to be equal for the cage and products, and A is the radius of the sphere. An analysis of reaction models with diffusion in an infinite medium showed that concentrations in the spot approach the steady state with a time dependence proportional to $t^{-0.5}$ (Crank 1975; Kiskin and Ogden 2001). Thus, the steady-state fluorescence at each laser power could be found from plots of fluorescence in $t^{-0.5}$ coordinates. At times $t > 1.75$ ms the fluorescence data were essentially linear with $t^{-0.5}$ (Fig. 4B). Data were fitted by regression lines in this interval to estimate the steady-state fluorescence from the intercepts with the ordinate as $t^{-0.5} \rightarrow 0$. The steady-state fluorescence was plotted as a function of the initial rate of photolysis (from GC model fits in Fig. 4A) and fitted with a hyperbolic curve (Eq. 4) to estimate the rate constant producing 50% photolysis in the steady state, $K_{0.5}$, as shown in Fig. 5B. To minimize complications due to bleaching, only data corresponding to laser powers up to 30 mW were used for fitting, covering initial photolysis rates up to 300 s^{-1}, and the maximum of the curve was constrained to 1.0. This gave an estimate for $K_{0.5}$ of 2530 ± 55 s^{-1}, which is an experimental estimate of the photolysis rate constant producing a half-maximal effect in the steady state, and is determined by the diffusion of cage and products and the spot geometry. The photolysis rate constants measured from the initial slopes (Fig. 5A) approach this value only at extremely high powers, >60 mW. Note also that the maximal fluorescence generated by laser photolysis saturates in the steady state at only 8–13% of the value observed in solutions subjected to complete near-UV photolysis (Fig. 5B). The reason for the apparent saturation at a low level is not known. It may be due to strong bleaching at high laser powers (see below) and/or to the presence of slow reaction steps in the photolysis mechanism, with diffusion of intermediates leading to substantial or even predominant generation of fluorescent product outside the spot. The steady-state fluorescence seen at rate constants of 300–1000 s^{-1} was slightly higher with high NPE-HPTS concentrations, but did not increase in proportion to the concentration. Furthermore, the normalized data were similar at pH 7 and pH 9.

Photolysis of NPE-HPTS measured in 4–20 μm diameter vesicles

Photolysis rates were also estimated by one-photon fluorescence measurements of total HPTS released by two-photon photolysis from NPE-HPTS inside impermeable vesicles (0.5 mM NPE-HPTS at pH 9). The two-photon fluorescence measurements of photolysis described above suggest that in brief laser exposures, duration ~ 10 μs, the rate of photolysis is unaffected by diffusion and cage depletion, and therefore provides a measure of the initial reaction rate. As the extent of product formation during a single short exposure was very low, thousands of 10 μs exposures were applied to accumulate detectable fluorescence. The interval

between exposures of ≥100 ms was long enough to allow the product and cage to redistribute uniformly over the whole vesicle, and also allowed "dark" reactions to proceed to completion. With this protocol, fluorescence in a vesicle plotted against cumulative laser exposure time would have a timecourse slower than the true photolysis reaction rate by the ratio V_s/V_{ves} because of the redistribution of the fluorescence (V_s is the two-photon volume, and V_{ves} is the vesicle volume). V_{ves} was calculated from the measured vesicle diameter assuming a sphere, and V_s was calculated for GL geometry estimated from the results of the Z-scans as described above (Eq. 2). The photolysis rate constants were recovered from the kinetics of the fluorescence increase seen in different size vesicles at different laser powers (3–5 vesicles for each laser power). The maximal level of fluorescence was measured after complete photolysis of NPE-HPTS in the same vesicle (see Methods and materials). Mean data from the measurements are shown in Fig. 5A. The photolysis rate constants showed a dependence on power, $k(P) = \gamma P^n$, where $n = 1.92 \pm 0.30$ for pooled data, very close to P^2. Constraining $n = 2$ we found $\gamma = 0.770 \pm 0.052$ s^{-1} mW^{-2}, estimated from fitting combined data (Fig. 5A, dotted line). Thus, the photolysis rate constants and the dependence on laser power obtained in these experiments were similar to the estimates obtained from the recordings directly from the two-photon focal volume. The rates estimated in the vesicle measurements with the pulse protocol used here are not subject to diffusional distortion by cage depletion or by diffusion of intermediates out of the spot, and are less affected by bleaching. Furthermore, the "dark" reactions should go to completion in the interval between consecutive 10 μs exposures and should not contribute to the observed rate. The rates estimated with this method are defined by light intensity, absorption and quantum efficiency of the cage, and the similarity between the results obtained with the two methods supports the idea that the initial excitation step determines the rate of two-photon photolysis of NPE-HPTS at the laser powers used here.

Two-photon excitation and multi-photon bleaching of HPTS fluorescence

The fluorescence and bleaching of photolysed NPE-HPTS by pulsed laser light were studied during the investigation of NPE-HPTS photolysis in order to normalize the data, and the results are given briefly here. Solutions containing NPE-HPTS concentrations of 5, 2 or 0.5 mM at pH 9, or 5 mM at pH 7, were photolysed in microcuvettes by exposure to near-UV light from a xenon flash lamp, and subsequently two-photon fluorescence was excited with 640 nm pulsed laser illumination. At laser powers exceeding 24 mW, the fluorescence showed substantial bleaching, with faster kinetics and larger magnitude as the laser power was increased (Figs. 3A, 6B). Furthermore, if the experiment was done in vesicles, bleaching of the fluorescence occurred without recovery. Thus the decline of fluorescence appears to be due to irreversible conversion of a fluorophore to a non-fluorescent form, and the process may be represented by a single-step irreversible reaction (as discussed in the preceding paper, Kiskin and Ogden 2001), described in the steady state by a relation similar to Eq. 4. The fluorescence in the laser spot should reach a steady state when the decrease due to bleaching is balanced by diffusion of the ground-state fluorophore into the laser spot from the surrounding solution. The normalized steady-state fluorescence, F_{ss}, was estimated from linear regression of the normalized fluorescence in $t^{-0.5}$ coordinates as before (Fig. 6A, 2 mM photolysed NPE-HPTS at pH 9) at times $t > 1.75$ ms.

The initial rate of bleaching was measured at the start of the illumination when depletion of the ground state fluorophore is negligible. Normalized fluorescence traces for each HPTS concentration were fitted by linear regression over the initial 10–70 μs for 54–72 mW and up to 100–300 μs for 24–48 mW laser power to yield apparent rate constants of bleaching, k_b, as shown in Fig. 6B. Regression lines fitted to double-logarithmic plots of the initial rate against laser power (solid and dashed lines, Fig. 6C) show that k_b depends on average laser power with slope n equal to 3.79 ± 0.26 at pH 9 or 3.80 ± 0.14 at pH 7. With the slope constrained to $n = 2$, no reliable fit to the data was obtained (Fig. 6C, dotted line). This indicates that although the fluorescence of HPTS under laser illumination is two-photon (Fig. 3B), the bleaching is three- or four-photon. The dimensions of effective multi-photon volumes for the bleaching reactions are thus even smaller than the two-photon focal volume V_s from which the fluorescence was recorded (see Xu and Webb 1997).

The steady-state fluorescence, F_{ss}, is plotted in Fig. 6D against the apparent rate constant of bleaching, k_b, obtained from the initial rates. The data are fitted by the relation predicted for a single-step irreversible bleaching reaction in two-photon volume:

$$F_{ss} = 1 - B_{max} k_b / (k_b + K_B) \quad (5)$$

where B_{max} is the maximal degree of bleaching at infinitely fast reaction and K_B is the apparent rate constant of the reaction producing half-maximal steady-state bleaching. Non-linear least-squares estimates gave final levels of F_{ss} at infinite laser power, $1–B_{max}$, of 0.657 ± 0.014 (pH 9) and 0.609 ± 0.014 (pH 7), significantly different from zero. These high residual levels of fluorescence may correspond to the fluorescence of HPTS present in the recording two-photon volume in diffusional exchange with a smaller internal 3–4 photon volume where bleaching occurs. Also, the volume difference scales down the rate constants of bleaching and the rate constant producing the half-maximal effect (analogous to $K_{0.5}$ in Eq. 4), estimated as $K_B = 453 \pm 61$ s^{-1} (at pH 9). This is much less than the $K_{0.5}$ estimated above for two-photon photolysis and may reflect the smaller volume of bleaching. For a further

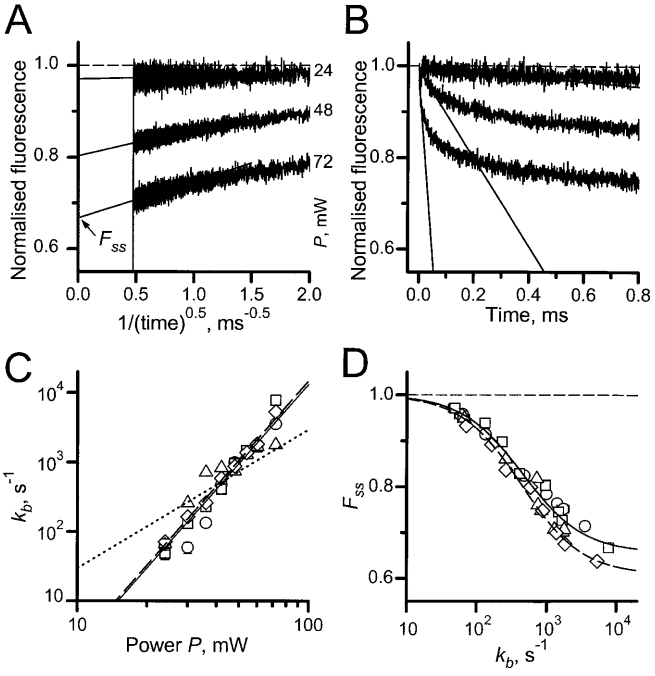

Fig. 6A–D Multi-photon bleaching of HPTS at high laser powers. **A** Fluorescence traces of Fig. 3A (2 mM photolysed NPE-HPTS solution, pH 9) normalized by peak fluorescence and plotted in $t^{-0.5}$ coordinates to show the approach to the steady state; average laser powers at the object were 24, 48 and 72 mW. *Lines* represent linear least-square fits to data obtained from times $t = 1.75$–1.8 ms to 4.4 ms. *Intercepts with ordinate* estimate the normalized steady-state fluorescence (F_{ss}, indicated by *arrow* at 72 mW). Note ordinate axis offset equals 0.55 in **A**, **B** and **D**. **B** Evaluation of initial kinetics of bleaching for the same data as in **A** plotted in linear coordinates. Apparent rate constants of bleaching, k_b, were found by linear fits to the initial region of the fluorescence traces (10 μs at 72 mW power to 300 μs at 24 mW). **C** The dependence of apparent initial rate constants of HPTS bleaching, k_b, on laser power, P; double logarithmic scale. Data symbols represent pH 9 (*circles*, 5 mM; *squares*, 2 mM; *triangles*, 0.5 mM) and pH 7 (*diamonds*, 5 mM) and apply to data shown in **C** and **D**. Standard deviations are shown where they exceed the symbol size. *Solid line*: linear fit to pooled data at pH 9 in logarithmic coordinates, slope $n = 3.79 \pm 0.26$, $\gamma = 3.54 \times 10^{-4}$; dashed line: fit at pH 7, $n = 3.80 \pm 0.14$, $\gamma = 3.73 \times 10^{-4}$. For comparison, the fit to all data at pH 9 with a fixed slope $n = 2$ is shown by the *dotted line*. **D** The dependence of normalized steady-state fluorescence (F_{ss}) on apparent rate constant of bleaching, k_b; semi-logarithmic scale. The *lines* are the least-square fits to the hyperbolic dependence $F_{ss} = 1 - B_{max} k_b / (k_b + K_B)$. The *solid line* is fitted to all data at pH 9, $B_{max} = 0.343 \pm 0.014$, $K_B = 453 \pm 61$ s^{-1}; *dashed line*: pH 7, $B_{max} = 0.391 \pm 0.014$, $K_B = 436 \pm 54$ s^{-1}

quantitative analysis of bleaching, the exact geometry of both two-photon and multi-photon volumes should be taken into account in the diffusion-reaction models.

Discussion

The aim of the experiments was to determine the maximum intensity of focused, pulsed near-IR laser irradiation that would be consistent with experiments in synaptic transmission, to obtain some idea of the processes involved in photodamage, and to measure the efficiency of two-photon photolysis of a representative near-UV cage at different laser powers to see the scale of improvement needed in two-photon photolysis cross-sections to make this approach useful.

Multiphoton damage to synaptic transmission

The tissue tolerance to pulsed laser light alone in a representative experimental protocol at the snake skeletal muscle endplate established an exposure limit of 5 mW average power (with the laser pulse parameters given) repetitively applied in 5 ms flashes at 1 Hz. In this protocol, over 600 exposures at 5 mW did not cause any changes in the recorded parameters. However, higher intensities of >6 mW produced a large increase in spontaneous synaptic activity in this protocol. A similar increase in mepp frequency can be seen with accidental mechanical damage, e.g. caused by the microelectrode to the terminal during recording. However, the photodamage seen here occurred at laser powers that were not obviously damaging to membranes in general, indicated for instance by the lack of effect on the muscle fibre membrane potential, and therefore the mechanism could be different from direct permeabilization of the presynaptic membrane. The heating of water by absorption of light is unlikely as a cause of damage since the temperature increase in the spot was calculated to be less than 0.2 °C (Schönle and Hell 1998), although the presence of cytosolic chromophores might contribute a larger change. Alternatively, the damage observed can be explained either by different susceptibility of pre- and postsynaptic membranes to pulsed laser illumination or by specific light absorption by a chromophore in the presynaptic terminal. Since Ca^{2+} influx through a damaged membrane will cause extensive exocytosis, Ca^{2+} influx induced by near-UV irradiation through a specific channel, described in cell lines by Mendez and Penner (1998), might be involved, although no effect of near-UV light itself delivered during flash photolysis experiments was seen in experiments in muscle, neuronal, liver or endothelial cells during the course of this study. Conclusions as to the presynaptic target of photodamage will require more experiments. However, comparison of the effects of the same energy dose per exposure, delivered either in short high-power or long low-power flashes, shows that multi-photon rather than single-photon absorption underlies this damage. Multiphoton damage at similar average powers and pulse parameters, but longer wavelength, has been reported in other neuronal cells by Koester et al. (1999) and Hopt and Neher (2001). The use of 640 nm here may be more damaging than the wavelengths >720 nm used in other studies, but the two-photon cross-sections of near-UV cages should also be higher at 640 nm, so the "safety factor" ratio of two-photon conversion to phototoxicity could in principle be better.

Changes were also seen in the appearance of irradiated boutons. At all powers tested there was uniform

bleaching of FM1-43 fluorescence, which after ~10 min of exposure affected the whole bouton. Only the small two-photon volume within the bouton was directly exposed to the laser and this observation therefore indicates a rapid cycling of vesicles through the two-photon region from other regions of the bouton at rest. FM1-43 bleaching was not a direct cause of photodamage, as laser powers < 5 mW produced bleaching without an increase in frequency of mepps and photodamage was still seen in boutons illuminated using > 5 mW laser powers without FM1-43 staining. However, it cannot be excluded that FM1-43 when present modified the photodamage.

Damage at average powers of 5–10 mW (König et al. 1997; Koester et al. 1999) and evidence of a two-photon mechanism of damage (Nichols and Webb 1998; Koester et al. 1999; König et al. 1999) were reported from studies of the effects of photodamage on the viability of cells in culture. Hopt and Neher (2001) describe experiments with a neurosecretory preparation more directly comparable with those reported here, which showed degranulation and elevated basal Ca^{2+} concentration in isolated chromaffin cells at similar low laser powers and with a similar strong dependence on pulse intensity, indicating multiphoton damage. Much higher average powers of 20–80 mW were used to elicit artificial Ca^{2+} spikes in cardiac myocytes with intracellular photolysis (Lipp and Niggli 1998), close to average powers reported to produce membrane damage in cardiac myocytes (Soeller and Cannell 1999). Data obtained in the course of our work also indicate that a small number (~10–20) of exposures to 18–24 mW were tolerated in HEK cells, dorsal root ganglion and liver cells, and membrane puncture was seen in muscle fibres at 24 mW with 1 s exposures. The susceptibility to photodamage of vesicular release in a synaptic preparation assayed over a long experiment may be expected to be greater than in short-term experiments or with simpler physiological processes. However, it is essential to ensure in each system studied that effects attributed to photolysis are not due to photodamage.

Assessment of photolysis

The rate of fluorescence production in femtolitre volumes of caged fluorophore solution provides a quantitative assay of photoconversion. NPE-HPTS used here has photochemistry representative of near-UV caged compounds used in biological applications (McCray and Trentham 1989; Corrie and Trentham 1993). The rate constant of two-photon photolysis of this compound at laser powers shown to be tolerated in synaptic experiments, ~5 mW, was estimated to be approximately 3 s^{-1} by extrapolation from data at high power. Because of diffusion, this rate is insufficient to produce a measurable change in concentration in the two-photon volume, either initially or in the steady state. Thus, a significant conclusion here is that two-photon photolysis of NPE-HPTS at physiologically acceptable laser powers is negligible. Similar results with two-photon photolysis have been reported for other widely used near-UV absorbing caged compounds such as DM-nitrophen and NP-EGTA (Brown et al. 1999).

Analysis of the NPE-HPTS photolysis at high laser powers was nevertheless carried out to develop a method suitable for other chromophores, to estimate the two-photon cross-section and determine the properties needed in a physiologically useful caged reagent. However, caged fluorophores have two photosensitive groups in the same molecule and these may interact, so the results should be applied with caution to caged compounds having a single chromophore. The structural changes responsible for uncaging the fluorescence and their place in the photoreaction cascade have to be identified and problems with fluorophore bleaching avoided.

Fluorescence and bleaching of HPTS

The peak fluorescence of the photolysis products, presumably mainly HPTS, was proportional to the square of the laser power, showing that two-photon absorption at 640 nm underlies the excitation of fluorescence in these experiments. However, at high laser power, multiphoton bleaching of the fluorophore released by photolysis is the major factor compromising a precise analysis of the photolysis reactions. The fast decline of HPTS fluorescence after the peak, corresponding to the bleaching process, is difficult to explain in terms of a single irreversible reaction, because the steady-state fluorescence does not decline to zero with increasing laser power ($B_{max} = 0.34$–0.39, Fig. 6D). The HPTS fluorophore is known to undergo complex bleaching reactions, with two successive photo-oxidative processes: absorption of the first photon excites the molecule, and a second photon deactivates it to an oxidized state with the release of an electron (Kotlyar et al. 1996). The third to fourth power dependence of the bleaching rate constant on the laser power seen here is generally compatible with such a complex mechanism, with two photons necessary to create an excited state and one or two photons to bleach it. A consequence of absorption of three or more photons for bleaching is that the reaction occurs in a small three- or four-photon volume enclosed inside a larger two-photon volume of fluorescence excitation and emission. As the fluorescence is collected from the larger two-photon volume containing diffusing HPTS, this may explain the apparent inability to completely bleach the dye even at "infinitely fast" bleaching. Bleaching of fluorophores in two-photon imaging with three-photon or higher order absorption has been reported by Patterson and Piston (2000).

Alternative explanations for the decline of the fluorescence may be ground state depletion and intersystem crossing (see Xu and Webb 1997). Finally, a further complication in interpretation may arise from the

proton sensitivity of HPTS fluorescence. Although 100 mM concentrations of pH buffer were present, local transient pH changes due to photolysis cannot be excluded. Thus, a more precise account of multi-photon bleaching of HPTS requires additional photochemical experiments.

NPE-HPTS photolysis reactions

The fluorescence traces obtained when NPE-HPTS was photolysed at low laser power showed a sigmoidal onset (Fig. 2, bottom traces). The initial slow component of the fluorescence change decreased in amplitude and eventually disappeared as the laser power increased. This suggests that the product release results from two or more sequential reactions, the rate of at least one increasing with laser power. The simplest explanation is a scheme with two sequential irreversible steps, one with a rate constant k_e which increases with laser power, and the second with a rate constant k_p independent of light. These steps have been tentatively assigned to the chromophore excitation and the "dark" reaction of product release, respectively (see Kiskin and Ogden 2001). A lower limit estimate of k_p can be made from the observation that photolysis rate constants increased up to 2190 s^{-1} without saturation at the maximum power used here (72 mW). As the overall rate constant cannot be higher than k_p, this implies that the "dark" reactions represented by k_p have rates >2190 s^{-1}.

The near-UV photochemistry of NPE-based caged compounds has been extensively studied. In the photolysis scheme elucidated for NPE-caged phosphates, *aci*-nitro intermediates form rapidly (rate $>10^5$ s^{-1}) after absorption of a near-UV photon, and a proton is released. The intermediates decay to products in a final irreversible reaction shown to be catalysed by protons (Walker et al. 1988). The rate of the final "dark" reaction in NPE-HPTS photolysis was found to be slow at pH values higher than 7 and increased in approximate proportion to $[H^+]$ (Jasuja et al. 1999), similar to the first-order dependence on proton concentration demonstrated for several NPE-caged compounds (e.g. McCray and Trentham 1989; Corrie et al. 1993; reviewed by Corrie and Trentham 1993). In contrast, two-photon photolysis of NPE-HPTS displayed no pH dependence in the pH range from 6 to 9, neither in the kinetics of fluorescence production nor in normalized steady-state photolysis with two-photon fluorescence excitation in the laser spot. The estimate of $k_p>2190$ s^{-1} for the "dark" reaction is much higher than expected from one-photon data, estimated as 550 s^{-1}at pH 7 and 16 s^{-1} at pH 9 (Jasuja et al. 1999). This raises the possibility that two-photon photolysis of NPE-HPTS involves photochemical reactions different from the one-photon scheme. An alternative explanation for the absence of pH dependence, and apparently high k_p, may be that the fluorescence recorded from the two-photon spot is due to fluorescent intermediates appearing before a final release of HPTS. In this case, a single-step reaction with a rate $k_e(P)$ can model the results, since the "dark" reaction (k_p) does not change the fluorescence and could be slow and pH sensitive. The results obtained with two-photon photolysis by cumulative 10 μs trains of laser pulses in Sylgard vesicles, with conventional single-photon excitation used for monitoring fluorescence, are influenced less by bleaching. Furthermore, the influence of diffusion on the photolysis rate is excluded by the very short 10 μs exposures, and any "dark" reactions with $k_p \approx 100$ s^{-1} are likely to be complete in the interval >100 ms between the 10 μs exposures. The apparent rate constants of NPE-HPTS photolysis estimated in vesicles therefore depend only on the excitation rate constant $k_e(P)$, determined by the two-photon absorption and quantum yield. The results were close to those obtained in the spot fluorescence measurements and displayed the same dependence on laser power (Fig. 5A), indicating that the initial photoactivation is rate limiting.

Calculation of two-photon photolysis cross-sections

The similarity in the photolysis rates estimated with spot and vesicle measurements suggests that the initial rate constants measured with both are estimates of the rate constants of cage excitation, k_e. Because excitation is produced by a train of laser pulses, of ~200 fs at 76 MHz, k_e depends on the excitation occurring during each pulse, determined by the two-photon photolysis cross-section $\delta = \sigma\eta$, where η is the quantum efficiency of photolysis and σ the two-photon absorption cross-section. It is therefore possible to estimate the two-photon photolysis cross-section of NPE-HPTS from the dependence of the photolysis rate constant on the average laser power, P. Equations relating these parameters are given in Appendix 1 (Eqs. A5 and A6). Since the excitation rate constants k_e showed approximate proportionality to the square of the average power, $k_e(P) = \gamma P^2$, the slopes γ fitted to the data of Fig. 5A can be used to estimate δ from Eq. (A6) of Appendix 1:

$$k_e = 1.17\delta \frac{T}{\tau_p} \left(\frac{\lambda}{\pi h c w_0^2} \right)^2 P_{av}^2 VF \qquad (6)$$

Substituting parameters $w_0 = 0.7$ μm, $\tau_p = 200$ fs, $T = 13.16$ ns, $\lambda = 640$ nm and $VF = 0.63$ for an axial cylinder of radius $w_0/2$ and length w_0 assumed in making the calculation (see Appendix 1), the values obtained are $\delta = 0.019$ and 0.036 GM (1 GM = 10^{-50} $cm^4 \times s$/photon) for measurements from the laser spot and in vesicles, respectively. These results are comparable with the photolysis action cross-sections $\delta = 0.013$ GM reported for DM-nitrophen and <0.01 for NP-EGTA ($\lambda = 720$ nm; Brown et al. 1999), but lower than 1.4 GM for a new caged calcium Azid-1 (700 nm; Adams et al. 1997; Brown et al. 1999) and ~1 GM for Bhc-glutamate (740 nm; Furuta et al. 1999).

Minimum photolysis two-photon cross-section

Since the maximum average power, P_{max}, that could safely be used at the synaptic terminal was about 5 mW, it is of interest to estimate the minimum photolysis cross-section necessary at this intensity to generate a photolysis rate sufficient to produce a 50% steady-state concentration change in the photolysis volume. The reaction rate required to produce 50% cage depletion is determined by diffusional exchange between the two-photon spot and the bulk medium. Assuming a sphere of radius $w_0/2$ submerged in an infinite medium, close in dimensions to the axial cylinder (radius $w_0/2$, length w_0) used above to calculate δ, the photolysis rate required for 50% depletion of the cage concentration is $K_{0.5} = 2.5D/(w_0/2)^2$ (Eq. 4; see Kiskin and Ogden 2001). For average laser power P_{max}, the two-photon cross section at 100% quantum efficiency, δ_{min}, can be calculated by rearranging Eq. (A6) of Appendix 1 with $k_e = K_{0.5}$:

$$\delta_{min} = 8.55\pi^2 h^2 c^2 \left(\frac{w_0}{\lambda}\right)^2 \frac{\tau_p}{T} \frac{D}{P_{max}^2 VF} \qquad (7)$$

Assuming that diffusion of NPE-HPTS is similar to HPTS with $D = 230$ μm^2/s, and for $w_0 = 0.7$ μm, substitution of numerical values gives $\delta_{min} = 8.84$ GM when $P_{max} = 5$ mW, a value which is larger than δ for caged compounds currently available. It should be noted that the photolysis rate required for 50% steady-state depletion of the cage depends on diffusion and, as a result, δ_{min} is also proportional to the diffusion coefficient. For example, at $D = 800$ μm^2/s, the diffusion coefficient for free aqueous diffusion of an amino acid neurotransmitter, δ_{min} should be 30.8 GM. On the other hand, the effective diffusion coefficient may be reduced by tortuosity in the extracellular environment and binding within the tissue, e.g. for $D = 100$ μm^2/s, δ_{min} is reduced to 3.84 GM. Furthermore, it should be noted that these are the action cross-sections assuming unit quantum yield. The absorbance cross-sections will need to be higher than this if the quantum yields are low.

"Dark" reaction rates

Diffusion of intermediates will result in the release of products outside the two-photon spot (Kiskin and Ogden 2001). For this reason, rates of "dark" reactions, $k_p \sim 10^4$–10^5 s^{-1}, are important in localizing high concentrations of the product within femtolitre illumination volumes. This limitation applies to most caged compounds, including the caged glutamate, Bhc-glutamate (Furuta et al. 1999), which has a large photolysis cross-section of approximately 1 GM, and therefore a high rate of excitation k_e compared with NPE-HPTS, but the glutamate release rate is limited by a decarboxylation step, shown in similar reactions to have a rate measured as 150 s^{-1} (21 °C, pH 7; Papageorgiou and Corrie 1997). Though due attention is paid to efficient two-photon absorption of potential caged compounds, the problems of slow "dark" reaction rates unfortunately often remain.

The results of photolysis rate measurements also give an estimate of 2530 s^{-1} for the parameter $K_{0.5}$ defining diffusional exchange of reagents with the bulk solution during NPE-HPTS photolysis experiments (Fig. 5B). If the spot can be approximated by an equivalent sphere, the radius would be $(2.5D/K_{0.5})^{0.5} = 0.48$ μm, a value falling between $w_R = 0.35$ μm and $w_Z = 2.47$ μm defined for the GC geometry. The maximal steady concentration of product averaged in the spot cannot exceed a proportion $1/(1 + K_{0.5}/k_e)$ of the bulk cage concentration (Eq. 4). Given that $k_e = 3.2$ s^{-1} for a laser power of 5 mW, an upper limit of the steady-state product concentration for two-photon photolysis of NPE-HPTS is only ~0.13%.

It can be concluded that for NPE-HPTS and, probably, for most current caged compounds used for single-photon photolysis utilizing nitrobenzyl or nitrophenyl photochemistry, the application of multi-photon photolysis methods is impractical due to extremely low cross-sections of two-photon absorption, discussed above, and hence very low rates of excitation at non-toxic intensities. The development of caged compounds with large two-photon cross-sections (e.g. Albota et al. 1998) will eventually help to overcome the present limitations.

Acknowledgements We thank Dr. David Trentham for support and discussion during this work, and for providing NPE-HPTS, and Dr. John Corrie for discussion and advice.

Appendix 1: excitation rate and the two-photon absorption cross-section

The rate of excitation in photolysis depends on the cross-section of two-photon absorption and the quantum yield of the chromophore, and on the laser beam parameters. The relation between these parameters can be derived in a similar way to an expression for two-photon fluorescence (Xu and Webb 1996, 1997) by relating the number of excited molecules N_e in volume V to the total number of molecules $N_t = C_0 N_A V$ (C_0 is the cage concentration, N_A is Avogadro's number). Two-photon extinction in dilute solution is assumed to be negligible. In a small differential volume dV the number of photons absorbed in a two-photon process during time dt can be expressed through the photon flux Φ per unit area and unit time (in terms of photon energy, $\Phi = I(r,z,t)\lambda/hc$ where h is Planck's constant, c is the speed of light) and the cross-section of two-photon absorption, σ:

$$dN_{abs} = \sigma \Phi^2 dN_t dt = \frac{\sigma I(r,z,t)^2 \lambda^2 C_0 N_A}{h^2 c^2} dV dt \qquad (A1)$$

The number of excited molecules formed in the volume V per pulse period T is half the number of photons absorbed:

$$N_e = N_{abs}/2 = \frac{\sigma\lambda^2 C_0 N_A}{2h^2c^2}\int_T I_0(t)^2 dt \int_V S(r,z)^2 dV \qquad (A2)$$

[spatial and temporal dependence of incident light are separated as $I(r,z,t) = I_0(t)S(r,z)$]. The integral on time includes the time-averaged square of the light intensity $\langle I_0^2(t)\rangle$, which may be expressed through the time-averaged light intensity $\langle I_0(t)\rangle$ by using the second-order temporal coherence factor $g^{(2)}$ (Xu and Webb 1996, 1997). For pulses with FWHM duration τ_p and sech^2 shape:

$$g^{(2)} = \left\langle I_0(t)^2 \right\rangle / \langle I_0(t)\rangle^2 = 0.587T/\tau_p \qquad (A3)$$

The average beam power P_{av} can be substituted for the average beam intensity using Eq. (1). The spatial integral in the expression for N_e requires the volume of photolysis, V, to be explicitly defined, since the result strongly depends on how this volume V overlaps with the highly non-uniform distribution of the squared light intensity. This volume is chosen to be a small cylinder of radius R and length L, coaxial with the axis z of light propagation and centred in the focus. Then the fraction $N_e/N_t = \alpha$ of molecules which absorb light in each laser pulse in this volume is:

$$\alpha = \frac{1.17\sigma\lambda^2 P_{av}^2 T^2}{\pi^2 h^2 c^2 \tau_p w_0^4} VF \qquad (A4)$$

where VF is the spatial integral of the light intensity over the photolysis volume divided by the volume of the cylinder, a unitless "volume fraction" function. It reflects the fraction of the two-photon spot volume V_s included inside the volume V. For large volumes V containing the whole spot, $VF = V_s/V$ (see Eq. 2). In the case of the coaxial cylinder defined above, VF can be written as:

$$VF = \frac{1}{V}\int_V S(r,z)^2 dV$$

$$= \frac{Z_R w_0^2}{2R^2 L}\left\{ atan\left(\frac{L}{2Z_R}\right) - \frac{1}{Z_R}\int_0^{L/2} \frac{exp\left[\frac{-4R^2}{w_0^2\left[1+(z/Z_R)^2\right]}\right]}{1+(z/Z_R)^2} dz \right\} \qquad (A5)$$

The values of VF depend mainly on the first term and approach 1 only for very small sub-femtolitre volumes around the spot centre. The simplest approximation for the focal volume is a small cylinder of radius $w_0/2$ and length w_0, so it is close to the sphere of radius $w_0/2$ and encloses the FWHM of intensity distribution section around the focal plane. The volume fraction function $VF(w_0)$ for this geometry (Eq. A5) can be approximately written as $VF(w_0) = 0.629[1-\exp(-w_0/0.0685\ \mu m)]$ for $w_0 > 0.04$ μm with no more than 3% error. At $w_0 > 0.3$ μm, VF can be regarded as constant at ~0.63, the value used in numerical calculations.

If the rate of product formation from the excited state is high, $k_p > 1/T$, all excited molecules convert to product in the interval T between laser pulses. In this case the rate of photolysis measures the rate of excitation, k_e. Also, in experiments in closed vesicles with repetitive 10 μs photolysing pulses, k_e is measured directly by fluorescence accumulation. The excitation rate is the fraction of molecules formed per single laser pulse, $k_e = \alpha\eta/T$ (see Kiskin and Ogden 2001), and is related to the photolysis two-photon cross-section, δ, by defining $\delta = \sigma\eta$ as the product of the absorption cross-section, σ, and the quantum efficiency, η. Substituting for α, the relation of k_e to δ from Eq. (A4) is:

$$k_e = 1.17\delta\frac{T}{\tau_p}\left(\frac{\lambda}{\pi h c w_0^2}\right)^2 P_{av}^2 VF \qquad (A6)$$

This expression provides a basis for the experimental determination of δ from the dependence of k_e on the square of the average power, using beam parameters determined independently.

Appendix 2: fluorescence and photolysis measurements with two-photon absorption described by a Gaussian cylinder distribution function

Let photolysis occur at a temporarily constant but spatially non-uniform rate described by the probability of two-photon absorption given by a GC function (Eq. 3):

$$K exp\left(-r^2/w_R^2\right) exp\left(-z^2/w_Z^2\right) \qquad (A7)$$

where K is the zero-order rate in the focus $r = 0$, $z = 0$. This condition approximates a first-order reaction with rate constant k, assuming that the concentration C_0 does not change with time, $K = kC_0$. The diffusional redistribution of the product concentration with time, $P(x,y,z,t)$, can be obtained by integration in Cartesian coordinates of an expression for a continuous unit point source (Carslaw and Jaeger 1959; eq. 10.2.2):

$$P(x,y,z,t) = \frac{K}{8(\pi D)^{1.5}} \times \int_0^t (t-\tau)^{-1.5} \int_{-\infty}^{\infty}\int_{-\infty}^{\infty}\int_{-\infty}^{\infty} \exp\left[-\frac{(x-p)^2+(y-q)^2+(z-s)^2}{4D(t-\tau)} - \frac{p^2+q^2}{w_R^2} - \frac{s^2}{w_Z^2} \right] dp\, dq\, ds\, d\tau \qquad (A8)$$

where D is the diffusion coefficient. To obtain the result of fluorescent measurements of product concentration from the whole volume, the distribution $P(x,y,z,t)$ should be integrated again with a corresponding non-uniform excitation function which in these experiments is the same GC function as for photolysis. The result should be normalized to the total amount of cage in the GC volume ($C_0\pi^{1.5}w_R{}^2 w_Z$). Switching to cylindrical coordinates, we will find that the kinetics of normalized fluorescence of product Fl is described by the integral:

$$Fl(t) = 2\pi \int_0^{\infty} \int_{-\infty}^{\infty} \int_0^{t} \frac{Kr \exp\left\{ \begin{array}{l} \frac{r^2 w_R^2}{4D(t-\tau)\left[w_R^2+4D(t-\tau)\right]} + \frac{z^2 w_Z^2}{4D(t-\tau)\left[w_Z^2+4D(t-\tau)\right]} - \frac{r^2+z^2}{4D(t-\tau)} \\ -\frac{r^2}{w_R^2} - \frac{z^2}{w_Z^2} \end{array} \right\}}{\pi^{1.5}\left[w_R^2 + 4D(t-\tau)\right]\sqrt{w_Z^2 + 4D(t-\tau)}} \, d\tau \, dz \, dr \quad \text{(A9)}$$

Characteristic radial and axial diffusion times, $\tau_R = {w_R}^2/D$ and $\tau_Z = {w_Z}^2/D$, may be defined for the Gaussian cylinder. Integration first on spatial coordinates and then on time gives the dependence of the time course of the fluorescence detected from the GC spot on the release rate constant K during photolysis:

$$Fl(t) = \frac{2^{-1.5} K \tau_R}{\sqrt{1-\tau_R/\tau_Z}} \times ln\left[\frac{\left(\sqrt{\tau_Z}+\sqrt{\tau_Z-\tau_R}\right)\left(\sqrt{\tau_Z+2t}-\sqrt{\tau_Z-\tau_R}\right)}{\sqrt{\tau_R(\tau_R+2t)}}\right] \quad \text{(A10)}$$

This expression was used for fitting the initial part of the fluorescence curves obtained when photolysis of NPE-HPTS was measured from the laser spot. An asymptotic expansion of this expression for large times is:

$$\frac{2^{-1.5} K \tau_R}{\sqrt{1-\tau_R/\tau_Z}} \ln\left(\frac{1+\sqrt{1-\tau_R/\tau_Z}}{\sqrt{\tau_R/\tau_Z}}\right) - 0.25 K \tau_R \sqrt{\frac{\tau_Z}{t}} + \frac{K\tau_R}{48}\left(1+2\frac{\tau_R}{\tau_Z}\right)\left(\frac{\tau_Z}{t}\right)^{1.5} + O\left(t^{-2.5}\right) \quad \text{(A11)}$$

The derivative of $Fl(t)$ on time at $t \to 0$ is $K/2^{1.5}$, as for the spherical Gaussian case (Kiskin and Ogden 2001). The first term of the expansion represents the steady-state value, depending on the shape of the spot, and the result displays $t^{-0.5}$ kinetics as equilibrium is approached.

References

Adams SR, Lev-Ram V, Tsien RY (1997) A new caged Ca^{2+}, azid-1, is far more photosensitive than nitrobenzyl-based chelators. Chem Biol 4:867–878

Albota M, Beljonne D, Brédas J-L, Ehrlich JE, Fu J-Y, Heikal AA, Hess SE, Kogej T, Levin MD, Marder SR, McCord-Maughon D, Perry JW, Röckel H, Rumi M, Subramaniam G, Webb WW, Wu X-L, Xu C (1998) Design of organic molecules with large two-photon absorption cross-sections. Science 281:1653–1656

Betz WJ, Bewick GS (1992) Optical analysis of synaptic vesicle recycling at the frog neuromuscular junction. Science 255:200–203

Brown EB, Shear JB, Adams SR, Tsien RY, Webb WW (1999) Photorelease of caged calcium in femtoliter volumes using two-photon excitation. Biophys J 76:489–499

Carslaw HS, Jaeger JC (1959) Conduction of heat in solids, 2nd edn. Oxford University Press, New York

Corrie JET, Trentham DR (1993) Caged nucleotides and neurotransmitters. In: Morrison H (ed) Bioorganic photochemistry, vol 2. Wiley, New York, pp 243–305

Corrie JET, DeSantis A, Katayama Y, Khodakhah K, Messenger JB, Ogden DC, Trentham DR (1993) Postsynaptic activation at the squid giant synapse by photolytic release of L-glutamate from a "caged" L-glutamate. J Physiol (Lond) 465:1–8

Crank J (1975) The mathematics of diffusion, 2nd edn. Oxford University Press, New York

Denk W (1994) Two-photon scanning photochemical microscopy: mapping ligand-gated ion channel distributions. Proc Natl Acad Sci USA 91:6629–6633

Fiekers JF (1983) Effects of the aminoglycoside antibiotics, streptomycin and neomycin, on neuromuscular transmission. I. Presynaptic considerations. J Pharmacol Exp Ther 225:487–495

Furuta T, Wang SS-H, Dantzker JL, Dore TM, Bybee WJ, Callaway EM, Denk W, Tsien RY (1999) Brominated 7-hydroxycoumarin-4-ylmethyls: photolabile protecting groups with biologically useful cross-sections for two-photon photolysis. Proc Natl Acad Sci USA 96:1193–1200

Guild JB, Xu C, Webb WW (1997) Measurement of group delay dispersion of high numerical aperture objective lenses using two-photon excited fluorescence. Appl Opt 36:397–401

Hopt A, Neher E (2001) Highly non-linear photodamage in two-photon fluorescence microscopy. Biophys J 80:2029–2036

Jasuja R, Keyoung J, Reid GP, Trentham DR, Khan S (1999) Chemotactic responses of *E. coli* to small jumps of photoreleased L-aspartate. Biophys J 76:1706–1719

Kiskin NI, Ogden DC (2001) Two-photon excitation and photolysis by pulsed laser illumination modelled by spatially non-uniform reactions with simultaneous diffusion. Eur Biophys J DOI 10.1007/s00249-001-0186-y

Kiskin NI, Trentham DR, Chillingworth R, McCray JA, Ogden D (1999) Pulsed laser light intensities producing photolysis by the two-photon effect damage presynaptic terminals of the snake endplate. J Physiol (Lond) 518:160P

Koester HJ, Baur D, Uhl R, Hell SW (1999) Ca^{2+} imaging with pico- and femtosecond two-photon excitation: signal and photodamage. Biophys J 77:2226–2236

König K, So PTC, Mantulin WW, Gratton E (1997) Cellular response to near-infrared femtosecond laser pulses in two-photon microscopes. Opt Lett 22:135–136

König K, Becker TW, Fischer P, Riemann I, Halbhuber KJ (1999) Pulse-length dependence of cellular response to intense near-infrared laser pulses in multi-photon microscopes. Opt Lett 24:113–115

Kotlyar AB, Borovok N, Raviv S, Zimanyi L, Gutman M (1996) Fast redox perturbation of aqueous solution by photoexcitation of pyranine. Photochem Photobiol 63:448–454

Lipp P, Niggli E (1998) Fundamental calcium release events revealed by two-photon excitation photolysis of caged calcium in guinea-pig cardiac myocytes. J Physiol (Lond) 508: 801–809

McCray JA, Trentham DR (1989) Properties and uses of photoreactive caged compounds. Annu Rev Biophys Biophys Chem 18:239–270

Mendez F, Penner R (1998) Near-visible ultraviolet light induces a novel ubiquitous calcium-permeable ion channel in mammalian cell lines. J Physiol (Lond) 507:365–377

Nichols JA, Webb WW (1998) Multi-photon microscopy – a tool to study photodamage. Biophys J 74:A189

Papageorgiou G, Corrie JET (1997) Synthesis and properties of carbamoyl derivatives of photolabile benzoins. Tetrahedron 53:3917–3932

Patterson GH, Piston D. (2000) Photobleaching in two-photon excitation microscopy. Biophys J 78:2159–2162

Schönle A, Hell SW (1998) Heating by absorption in the focus of an objective lens. Opt Lett 23:325–327

Soeller C, Cannell MB (1999) Two-photon excited flash photolysis for the study of model cell systems. Biophys J 76:A307

Svoboda K, Tank DW, Denk W (1996) Direct measurement of coupling between dendritic spines and shafts. Science 272:716–719

Walker JW, Reid GP, McCray JA, Trentham DR (1988) Photolabile 1-(2-nitrophenyl)ethyl phosphate esters of adenine nucleotide analogues; synthesis and mechanism of photolysis. J Am Chem Soc 110:7170–7177

Xia P, Bungay PM, Gibson CC, Kovbasnjuk ON, Spring KR (1998) Diffusion coefficients in the lateral intracellular spaces of Madin-Darby canine kidney cell epithelium determined with caged compounds. Biophys J 74:3302–3312

Xu C, Webb WW (1996) Measurement of two-photon excitation cross sections of molecular fluorophores with data from 690 to 1050 nm. J Opt Soc Am B 13:481–491

Xu C, Webb WW (1997) Multiphoton excitation of molecular fluorophores and nonlinear laser microscopy. In: Lakowicz JR (ed) Topics in fluorescence spectroscopy, vol 5. Plenum Press, New York, pp 471–540